Robust Automatic Steering Control for Look-Down Reference Systems with Front and Rear Sensors

Jürgen Guldner , Wolfgang Sienel , Han-Shue Tan,*
Jürgen Ackermann†, Satyajit Patwardhan, and Tilman Bünte†*

Abstract— **This paper describes a robust control design for automatic steering of passenger cars. Previous studies [1–3] showed that reliable automatic driving at highway speed may not be achieved under practical conditions with look-down reference systems which use only one sensor at the front bumper to measure the lateral displacement of the vehicle from the lane reference. An additional lateral displacement sensor is added here at the tail bumper to solve the automatic steering control problem. The control design is performed stepwise: First, an initial controller is determined using the parameter space approach in an invariance plane. This controller is then refined to accommodate practical constraints and finally optimized using the multi-objective optimization program MOPS. The performance and robustness of the final controller was verified experimentally at California PATH in a series of test runs.**

Keywords: Automotive, Robust Control, Automatic Steering

I. Introduction

Automatic steering control is a vital component of highway automation, currently investigated worldwide in several programs, e.g. NAHSC in the US (see e.g. [4]) and ASV, SSVS and ARTS under ITS Japan [5]. Previous approaches can be grouped into *look-ahead* and *look-down* reference systems, according to the point of measurement of the vehicle lateral displacement from the lane reference. Look-ahead systems replicate human driving behavior by measuring the lateral displacement *ahead* of the vehicle. A number of research groups have successfully conducted experiments up to highway speed with look-ahead systems like machine vision or radar. Examples are VaMoRs-P [6], VITA-I and II [7, 8] and related projects within the European PROMETHEUS Program, Carnegie Mellon University's PANS [9], and California PATH's stereo-vision based system [10]. In an effort to remedy the susceptibility of machine vision to variation of light and weather conditions, radar reflective stripes with look-ahead capability have been developed and tested at The Ohio State University (OSU) [11].

Look-down reference systems, on the other hand, measure the lateral displacement at a location within or in the close vicinity of the vehicle boundaries, typically straight *down* from the front bumper. Examples include electric wire [12, 13] and magnetic marker reference systems [14]. Look-down reference systems are favorable due to their reliability, invariance to weather conditions and absence of occlusion by preceding vehicles. Despite an impressive amount of literature on theoretical control designs, most experimentally verified designs of look-down systems were restricted to low speed of less than 20 m/s (72 km/h, approx. 45 mph) under practical constraints such as actuator bandwidth limitations, sensor noise, passenger comfort, and stringent accuracy requirements. We have shown in [1, 2] that the extension of look-down systems to practical conditions of an Automated Highway System (AHS) environment with speeds above 30 m/s (108 km/h, approx. 67.5 mph) is nontrivial and requires complete re-thinking of the approach.

A promising approach is to add a second sensor to measure lateral vehicle displacement from the lane reference at the tail bumper. This provides a number of possible control design directions [3], e.g. feedback of angular displacement in addition to feedback of lateral displacement at the front bumper. Alternatively, this paper pursues a direct control design by re-writing the linearized dynamic equations in terms of front and tail lateral displacement and their derivatives. A block diagram of the new controller structure is shown in Figure 1. After describing the problem in Section II for a generic look-down reference system, the parameter space approach in an invariance plane is used in Section III to determine an initial robust controller based on state feedback. Refinement of the controller in Section IV derives an implementable output feedback controller version, considering the various practical constraints and limitations known to have impaired previous designs [3]. The control design is shown to exhibit the desired performance in experiments with one of the California PATH test cars.

II. Problem Description

A sketch of a vehicle following a lane reference is shown in Figure 2. The vehicle is depicted as a so-called single track model, which is obtained by lumping the two wheels of each axle into one wheel at the centerline of the vehicle. For the augmented look-down reference system as considered here, lateral displacement of the vehicle from the lane reference is measured both at the front (Δy_S) and at the tail (Δy_T) bumper. The displacement sen-

California PATH, University of California at Berkeley, Institute of Transportation Studies, 1357 S. 46th Street, Richmond, CA 94804-4698, USA, (hstan@path4.its.berkeley.edu)

Inst. for Robotics and System Dynamics, DLR Oberpfaffenhofen, Postfach 1116, D-82330 Weßling, Germany, (Wolfgang.Sienel@dlr.de)

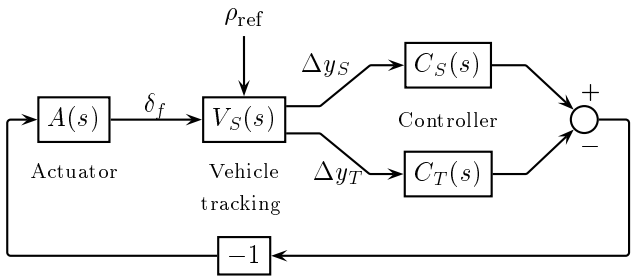

Fig. 1. Block diagram of controller using front and tail lateral displacement measurements

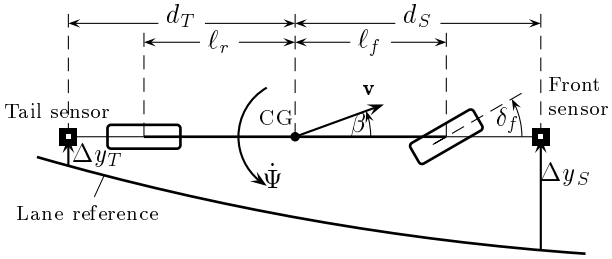

Fig. 2. Single track model for automatic tracking

sors are mounted at d_S in front of and d_T behind the center of gravity (CG) and are technology independent for the purpose of control design. The reference lane is assumed to consist of circular arcs with curvature ρ_{ref} as it is the case for US highways. Other vehicle parameters in Figure 2 are the distances ℓ_f and ℓ_r of front and rear axles from CG. The two vehicle dynamic states are also shown: vehicle side slip angle β between the velocity vector $\mathbf{v}$ (magnitude $v = |\mathbf{v}|$) and the longitudinal axis, and vehicle yaw rate $\dot{\Psi}$. The front wheel steering angle δ_f is the input of the automatic steering system.

A linearized state-space model of the lateral vehicle dynamics and the dynamics of front and tail lateral displacement from the lane reference is derived from the model in [15] as

$$\begin{bmatrix} \Delta\dot{y}_S \\ \Delta\ddot{y}_S \\ \Delta\dot{y}_T \\ \Delta\ddot{y}_T \end{bmatrix} = \begin{bmatrix} 0 & 1 & 0 & 0 \\ a_{21} & a_{22} & -a_{21} & a_{24} \\ 0 & 0 & 0 & 1 \\ a_{41} & a_{42} & -a_{41} & a_{44} \end{bmatrix} \begin{bmatrix} \Delta y_S \\ \Delta\dot{y}_S \\ \Delta y_T \\ \Delta\dot{y}_T \end{bmatrix} + \begin{bmatrix} 0 & 0 \\ b_2 & -v^2 \\ 0 & h_4 v \\ b_4 & -v^2 \end{bmatrix} \begin{bmatrix} \delta_f \\ \rho_{ref} \end{bmatrix} \quad (1)$$

with

$$\begin{aligned} a_{21} &= \frac{h_2}{M h_4} - \frac{d_S h_1}{I_\Psi h_4} \\ a_{41} &= \frac{h_2}{M h_4} + \frac{d_T h_1}{I_\Psi h_4} \\ a_{22} &= \frac{h_1 - d_T h_2}{M v h_4} + \frac{d_S(d_T h_1 - h_3)}{I_\Psi v h_4} \\ a_{42} &= \frac{h_1 - d_T h_2}{M v h_4} - \frac{d_T(d_T h_1 - h_3)}{I_\Psi v h_4} \\ a_{24} &= -\frac{h_1 + d_S h_2}{M v h_4} + \frac{d_S(d_S h_1 + h_3)}{I_\Psi v h_4} \\ a_{44} &= -\frac{h_1 + d_S h_2}{M v h_4} + \frac{d_T(d_S h_1 + h_3)}{I_\Psi v h_4} \\ b_2 &= \mu c_f \left(\frac{1}{M} + \frac{d_S \ell_f}{I_\Psi}\right) \\ b_4 &= \mu c_f \left(\frac{1}{M} - \frac{d_T \ell_f}{I_\Psi}\right) \end{aligned}$$

and auxiliary variables

$$\begin{aligned} h_1 &= \mu(c_r \ell_r - c_f \ell_f) & h_2 &= \mu(c_f + c_r) \\ h_3 &= \mu(c_r \ell_r^2 + c_f \ell_f^2) & h_4 &= d_S + d_T \end{aligned}$$

M denotes the total vehicle mass and I_Ψ is the total yaw moment of inertia. The parameters c_f and c_r are the cornering stiffnesses of front and rear tires, respectively, with μ being the road adhesion factor. The subsequent control design is based on the parameters of one of the experimental vehicles used at California PATH, a 1986 Pontiac 6000 STE sedan, summarized in Table 1. All parameters are constant or slowly time varying during an operation and hence are assumed to be known e.g. by estimation, except for the road adhesion factor μ, which may change abruptly while driving.

Practical realization of an automatic steering system requires a steering actuator to generate the front steering angle δ_f. In view of a serial production, a low-prize solution, i.e. a low-bandwidth actuator is desirable. With decreasing actuator bandwidth, however, the actuator dynamics become more and more crucial for stability of the closed loop system and interfere with control design. Consequently, the actuator dynamics have to be considered already in the control design phase. In order to avoid excitation and saturation of nonlinear actuator dynamics, the bandwidth of the controller should remain below the linear approximation of the actuator bandwidth. Various experiments led to the formulation of a linearized, third order low pass actuator model, with a complex pole pair at 5 Hz with 0.4 damping, and a third pole at 10 Hz for the actuator of the Pontiac 6000 STE.

Performance requirements and practical constraints, discussed in detail in [1–3], include:

M	I_Ψ	ℓ_f	ℓ_r	d_S	d_T	$c_f = c_r$
1573 kg	2873 kg m^2	1.1 m	1.58 m	1.96 m	2.49 m	80000 N/rad

TABLE I
VEHICLE PARAMETERS OF A 1986 PONTIAC 6000 STE SEDAN

- The automatic steering control should to be robust with respect to changing road adhesion for a range from good road with $\mu = 1$ to poor, e.g. wet and slippery road surface with $\mu = 0.5$. Robustness with respect to μ is vital due to abrupt transitions.
- The maximum lateral displacement for responses to step inputs of road curvature $\rho_{\text{ref}} = a_{\text{ref}}/v^2$ equivalent to reference lateral acceleration of $a_{\text{ref}} = 0.1$ g should be less than 0.15 m during normal operation with $\mu = 1$ and no more than 0.30 m in extreme cases $\mu = 0.5$, without overshoot and up to $v = 40$ m/s.
- Passenger comfort should be similar to manually steered cars, requiring closed loop damping at least as good as in conventional cars and the ability to compromise between accuracy and ride comfort in the control design.

III. Robust Control Design

A closer look at the vehicle model (1) reveals that the eigenvalues can be separated into two groups: Group one, a pair of complex conjugate poles, which stems from the lateral dynamics of the vehicle model; the second group consists of a double pole at the origin from integrating $\Delta\dot{y}_S$ and $\Delta\dot{y}_T$. Since the dynamics of the complex pole pair are well-behaved and sufficiently damped, their original locations should be preserved in closed loop. This holds also for the actuator poles. The controller should only shift the double integrator poles to guarantee sufficient performance and robustness of the automatic steering system. These design objectives can be accomplished by the parameter space approach in an invariance plane. This concept was also discussed in [16] for the automatic steering problem. However, since not all design specifications can be considered in this approach, the initial control design will be refined in Section IV for practical implementation.

A. Design in an Invariance Plane

For an introduction to the design approach in an invariance plane (see [15] for details), assume a genuine n th-order state space model $\dot{\boldsymbol{x}} = \boldsymbol{A}\boldsymbol{x} + \boldsymbol{b}u$ with proportional state-feedback control $u = -\boldsymbol{k}^T\boldsymbol{x}$. This approach allows to determine an m-dimensional subspace in the n-dimensional controller parameter space, such that only m specific eigenvalues of the given plant are shifted by arbitrary selection of controller gains $\boldsymbol{k}$ from this subspace, while the remaining $n - m$ eigenvalues remain at their original locations. This approach is based on Ackermann's Formula [15]:

Theorem (Ackermann): For a controllable single input system $(\boldsymbol{A}, \boldsymbol{b})$, the feedback vector

$$\boldsymbol{k}^T = \boldsymbol{e}^T p(\boldsymbol{A}) \tag{2}$$

with

$$\boldsymbol{e}^T = \begin{bmatrix} 0 & 0 & \dots & 1 \end{bmatrix} \begin{bmatrix} \boldsymbol{b} & \boldsymbol{A}\boldsymbol{b} & \dots & \boldsymbol{A}^{n-1}\boldsymbol{b} \end{bmatrix}^{-1} \tag{3}$$

assigns the eigenvalues of $\boldsymbol{A} - \boldsymbol{b}\boldsymbol{k}^T$ to the roots of the polynomial $p(s)$.

The desired characteristic closed loop polynomial $p(s)$ is now written as a product $p(s) = h(s) \cdot t(s)$, where $h(s)$ represents the eigenvalues which remain fixed and $t(s)$ denotes the eigenvalues to be shifted. Equation (2) becomes

$$\boldsymbol{k}^T = \boldsymbol{e}^T h(\boldsymbol{A}) t(\boldsymbol{A}) = \boldsymbol{e}_h^T t(\boldsymbol{A}), \tag{4}$$

where $\boldsymbol{e}_h^T = \boldsymbol{e}^T h(\boldsymbol{A})$. Further assuming that only two eigenvalues should be shifted at a time, i.e. $t(s) = t_0 + t_1 s + s^2$, equation (4) yields

$$\boldsymbol{k}^T = \boldsymbol{e}_h^T (t_0 \boldsymbol{I} + t_1 \boldsymbol{A} + \boldsymbol{A}^2) = [t_0 \;\; t_1 \;\; 1] \begin{bmatrix} \boldsymbol{e}_h^T \\ \boldsymbol{e}_h^T \boldsymbol{A} \\ \boldsymbol{e}_h^T \boldsymbol{A}^2 \end{bmatrix}. \tag{5}$$

For the open loop, i.e. $\boldsymbol{k}^T = \boldsymbol{0}^T$, the eigenvalues represented by $t(s)$ are denoted by $d(s) = d_0 + d_1 s + s^2$, i.e.

$$\boldsymbol{0}^T = \boldsymbol{e}_h^T d(\boldsymbol{A}) = \boldsymbol{e}_h^T (d_0 \boldsymbol{I} + d_1 \boldsymbol{A} + \boldsymbol{A}^2). \tag{6}$$

Forming the difference of (4) and (6) yields

$$\boldsymbol{k}^T = [\kappa_a \;\; \kappa_b] \begin{bmatrix} \boldsymbol{e}_h^T \\ \boldsymbol{e}_h^T \boldsymbol{A} \end{bmatrix}, \tag{7}$$

with $\kappa_a = t_0 - d_0$ and $\kappa_b = t_1 - d_1$. By arbitrary (κ_a, κ_b) a feedback vector $\boldsymbol{k}^T$ is determined in the two-dimensional cross-section defined by the vectors $\boldsymbol{e}_h^T$ and $(\boldsymbol{e}_h^T \boldsymbol{A})$ such that only the two eigenvalues of $d(s)$ are shifted while $h(s)$ remains fixed.

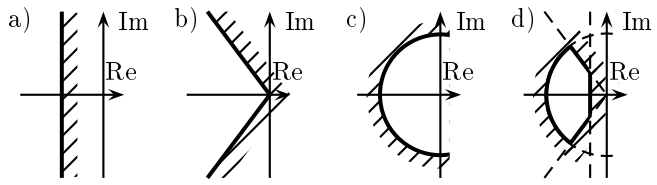

Fig. 3. Basic elements of Γ-stability: (a) settling time, (b) damping, (c) bandwidth. The combination of these basic elements (d) allows to fulfill several basic conditions simultaneously.

The parameters (κ_a, κ_b) could now be determined for a nominal plant such that the poles of $d(s)$ are located at a desired position in the eigenvalue plane. This pole-placement approach, however, is a very strong condition and does not allow to incorporate any other requirements, for example robustness for other operating points diverging from the nominal operating point. A more flexible approach is to determine the set of parameters in the (κ_a, κ_b)-plane, for which the system is robustly stable. This can be accomplished by the parameter space approach to be discussed below.

B. Parameter Space Approach

In order to satisfy the performance requirements, especially with respect to passenger comfort, plain Hurwitz stability is not sufficient. Hence, the notion of Γ-stability is introduced, where Γ describes a subset of the left half of the eigenvalue plane. A suitable region Γ is defined by the control engineer according to the system specifications. This allows to consider certain specifications like settling time, damping, and bandwidth, see Figure 3. A system is called Γ-stable, if its eigenvalues are entirely contained in the region Γ.

The task is now to determine the set of (κ_a, κ_b)-parameters for which the nominal system is Γ-stable. This problem can be solved using the parameter space approach [15]. The boundary $\partial\Gamma$ of the region Γ is mapped into the (κ_a, κ_b)-plane via the characteristic polynomial $p(s, \kappa_a, \kappa_b)$ by separating it into real and imaginary parts for a grid point $s^* = \sigma^* + \omega^*$ on the boundary $\partial\Gamma$ and solving the set of equations

$$\begin{aligned} \mathrm{Re}\, p(\sigma^* + \omega^*, \kappa_a, \kappa_b) &= 0 \\ \mathrm{Im}\, p(\sigma^* + \omega^*, \kappa_a, \kappa_b) &= 0 \end{aligned} \tag{8}$$

for κ_a and κ_b. Solution of the set of equations in (8) along the boundary $\partial\Gamma$ yields the Γ-stability boundaries in the (κ_a, κ_b)-plane. These boundaries divide the plane into a finite number of regions. By checking Γ-stability of an arbitrary point of each region, the set of Γ-stabilizing gains (κ_a, κ_b) can be determined easily.

C. Simultaneous Γ-Stabilization in an Invariance Plane

In the case of an uncertain plant, the characteristic polynomial depends also on the uncertain parameters $\boldsymbol{q} = [q_1\ q_2\ \ldots\ q_\ell]^T$. Since in general, it is not possible to design a controller considering the entire operating domain

$$Q = \{\boldsymbol{q} \mid q_i \in [q_i^-;\, q_i^+],\ i = 1, 2, \ldots, \ell\}$$

in one single design step, a more practically oriented way is chosen: A finite number of representatives of the plant, e.g. the vertices of the operating domain Q, is selected and a controller is designed which simultaneously Γ-stabilizes those representatives. Using the parameter space approach, the set of Γ-stabilizing gains is determined for each representative and finally the intersection of the sets is formed. Controllers out of this resulting set will Γ-stabilize all given representatives. A subsequent analysis of the closed loop has to verify Γ-stability for the entire operating domain Q.

This approach of simultaneous Γ-stabilization for uncertain plants can be combined with the design in an invariance plane, if such a plane is determined adequately for a nominal operating point $\boldsymbol{q}_0$ and the Γ-stability boundaries for all representatives are displayed in this specific plane. For a general operating point $\boldsymbol{q} \neq \boldsymbol{q}_0$ all eigenvalues (instead of only the selected ones) will be shifted since the invariance plane was especially determined for $\boldsymbol{q}_0$. However, for a reasonable choice of $\boldsymbol{q}_0$, for example the center of the operating domain Q, the deviation of the eigenvalues represented by $h(s, \boldsymbol{q})$ can be expected to be minor for plants not exhibiting extreme dynamic variations within Q.

An additional problem arises for automatic steering control: due to the actuator dynamics, pure state-feedback is not available as required for the invariance plane approach since only the vehicle states in (1) can be fed back. Thus, an invariance plane can not be determined for the full system comprising vehicle and actuator dynamics. A reasonable compromise is to neglect the actuator dynamics for the calculation of the invariance plane, but to include them in the parameter space approach when checking robust Γ-stability later.

Since control design for automatic steering is most difficult for high speed, the initial design will be carried out for maximal speed $v^+ = 40$ m/s. The only vehicle parameter assumed uncertain is road adhesion $\mu \in [0.5;\ 1]$. An invariance plane is calculated for an average road adhesion of $\mu_0 = 0.75$ at $v^+ = 40$ m/s for the system without actuator dynamics. The plane is determined such that only the double pole at the origin is shifted for the nominal plant, i.e. $d(s) = s^2$. The result for the data of

the Pontiac 6000 STE (see Table 1) is

$$\boldsymbol{k}^T = [\kappa_a \ \kappa_b] \begin{bmatrix} 12.35 & 0.15 & -5.39 & 0.66 \\ 15.06 & 12.01 & -15.06 & -6.73 \end{bmatrix} 10^{-3} \quad (9)$$

A hyperbola with a damping factor of $D = 0.4$ and maximal real part of $\sigma_0 = -0.5$ is selected as the Γ-stability boundary . The relatively low damping had to be chosen to allow incorporation of the actuator poles with damping $D_{act} = 0.4$. Equation (9) prescribes the (κ_a, κ_b)-plane in which the Γ-stability boundaries will be calculated for the system including the actuator for the two representatives $\mu^- = 0.5$ and $\mu^+ = 1$. The result is displayed in Figure **??**, with the region of simultaneous Γ-stabilization being the labeled triangle with corners (1, 2.5), (3, 5.8), and (35, 6.9). All controller gains (κ_a, κ_b) from this region guarantee Γ-stability for both representatives μ^- and μ^+. [1]

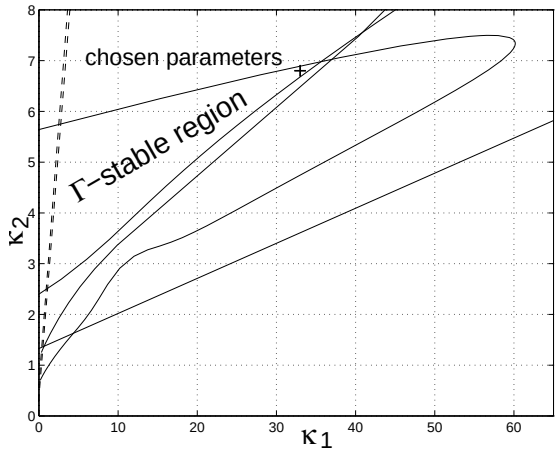

Fig. 4. Γ-stability boundaries in the (κ_a, κ_b)-plane for the two representatives

An adequate controller has now to be selected from the Γ-stable set. In order to achieve the tight accuracy requirements, a high gain solution obviously is a favorable choice. Such a solution with $\kappa_a = 33$ and $\kappa_b = 6.8$ is marked in Figure **??** with a small '+'. The resulting feedback vector $\boldsymbol{k}^T$ is

$$\boldsymbol{k}^T = \begin{bmatrix} 0.510 & 0.087 & -0.280 & -0.024 \end{bmatrix}. \quad (10)$$

In Table 2, a comparison of open loop and closed loop eigenvalues is shown. It reveals that only the open loop eigenvalues at the origin (integrators) are shifted significantly while the deviation of the other eigenvalues is minor.

[1] The calculation of the invariance plane and computation of Γ-stability boundaries were performed with PARADISE, a new toolbox for robust parametric control design. For more information, please visit the Web pages at `http://www.op.dlr.de/FF-DR-RR/paradise`.

From the state feedback vector $\boldsymbol{k}^T = [k_1 \ k_2 \ k_3 \ k_4]$ in (10), two controllers $C_S(s)$ and $C_T(s)$ are derived for the two measurements Δy_S and Δy_T, i.e.

$$C_S(s) = k_1 + k_2 s \quad \text{and} \quad C_T(s) = k_3 + k_4 s, \quad (11)$$

where s denotes the Laplace variable. A schematic block diagram of this controller structure was shown in 1.

IV. Controller Refinement

The state feedback controller designed above using the parameter space approach provides a good baseline for practical control design due to its inherent robustness and selective modification of poles in closed loop. Implementation, however, requires refinement to accommodate practical constraints and limitations. The objectives for refinement are:

- to obtain an implementable, output feedback controller version without feedback of the unmeasurable rates of lateral displacement, $\Delta\dot{y}_S$ and $\Delta\dot{y}_T$;
- to fulfill the performance requirements under the practical constraints listed in Section II;
- to achieve zero steady state error during curve riding;
- and to preserve the established characteristics of the initial design in terms of Γ-stability and robustness.

This step of controller refinement relies entirely on engineering practice and is based on time domain, eigenvalue and frequency domain considerations.

A. Modification of Controller Structure

No measurement of the *rate* of lateral displacement is available for most reference systems. Numerical differentiation is required to obtain derivative information for $\Delta\dot{y}_S$ and $\Delta\dot{y}_T$, e.g. in the form of lead filters of PDT_1-type instead of (11),

$$\begin{aligned} C_S(s) &= \frac{K_{D_S} s + K_{P_S}}{T_S s + 1}, \\ C_T(s) &= \frac{K_{D_T} s + K_{P_T}}{T_T s + 1}, \end{aligned} \quad (12)$$

with K_{D_S} and K_{D_T} being the D-gains k_2 and k_4, and K_{P_S} and K_{P_T} being the P-gains k_1 and k_3 of the initial control design (11), and the time constants T_S and T_T chosen sufficiently large. Full differentiation action, i.e. 90^o phase lead in $C_S(s)$ and $C_T(s)$ is only achieved for $T_S \ll (K_{D_S}/K_{P_S})$ and $T_T \ll (K_{D_T}/K_{P_T})$, colliding with noise considerations and actuator bandwidth limitations. A second order lead filter of PDD^2T_2-type, however, may achieve 90^o phase lead and also provides an additional degree of freedom for control design. Hence a suitable

$\mu^- = 0.5$		$\mu^+ = 1$	
open loop	closed loop	open loop	closed loop
$\omega_{1,2} = 0$ (integrators)	$\omega_{1,2} = 9.16$, $D_{1,2} = 0.92$	$\omega_{1,2} = 0$ (integrators)	$\omega_{1,2} = 5.98$, $D_{1,2} = 0.42$
$\omega_{3,4} = 4.44$, $D_{3,4} = 0.58$	$\omega_{3,4} = 4.76$, $D_{3,4} = 0.58$	$\omega_{3,4} = 2.87$, $D_{3,4} = 0.45$	$\omega_{3,4} = 2.83$, $D_{3,4} = 0.43$

TABLE II

LOCATIONS OF THE FOUR VEHICLE POLES IN OPEN AND CLOSED LOOP

controller structure is

$$\begin{aligned} C_S(s) &= \frac{K_{DD_S}s^2 + K_{D_S}s + K_{P_S}}{s^2/\omega_1^2 + 2D_S/\omega_1 s + 1}, \\ C_T(s) &= \frac{K_{DD_T}s^2 + K_{D_T}s + K_{P_T}}{s^2/\omega_1^2 + 2D_T/\omega_1 s + 1}. \end{aligned} \tag{13}$$

During *steady state* curve riding, the vehicle longitudinal axis is at an angle $\Delta\Psi_{ss} \neq 0$ to the tangent of the reference path, which is the natural side slip angle during steady state cornering. Consequently, only a single point along the longitudinal vehicle axis, Z at d_Z from CG, may achieve zero steady state tracking with $\Delta y_{Z_{ss}} = 0$; all other points P at $d_P \neq d_Z$ from CG will feature an offset of $\Delta y_{P_{ss}} \approx (d_Z - d_P)\Delta\Psi_{ss}$. Zero steady state tracking at Z (with $d_Z > 0$ for Z in front of CG) may be achieved by additional integral feedback of Δy_Z,

$$\frac{K_I}{s}\Delta y_Z = \frac{K_I}{s}\left(\frac{d_Z + d_T}{d_S + d_T}\Delta y_S + \frac{d_S - d_Z}{d_S + d_T}\Delta y_T\right). \tag{14}$$

For convenience of passengers, most likely observing tracking at the front end of the car, $d_Z = d_S$ is selected here.

Noise in lateral displacement measurements Δy_S and Δy_T should not be allowed to propagate through the closed loop. Besides the need to provide good damping at all frequencies to prevent excitation of a single noise frequency, controller roll-off is required to protect the actuator from high frequency noise. A third pole is added to (13) and hence with (14),

$$\begin{aligned} C_S(s) &= \frac{K_{DD_S}s^2 + K_{D_S}s + K_{P_S}}{(s/\omega_2 + 1)(s^2/\omega_1^2 + 2D/\omega_1 s + 1)} + \frac{K_I}{s}, \\ C_T(s) &= \frac{K_{DD_T}s^2 + K_{D_T}s + K_{P_T}}{(s/\omega_2 + 1)(s^2/\omega_1^2 + 2D/\omega_1 s + 1)}. \end{aligned} \tag{15}$$

is the final controller structure.

B. Choice of Controller Parameters

The parameters for the new controller structure in (15) are chosen sequentially. First, the denominator poles are determined as $\omega_1 = \omega_2 = 2\pi \cdot 2$ Hz, a bandwidth slightly below to the actuator bandwidth. This choice is a trade-off between the anticipated closed loop bandwidth and the need to avoid high frequency excitation of the actuator. Damping D is set to 0.8 to moderate the poor actuator damping of $D_{act} = 0.4$.

Second, the zeros and the steady state gains of $C_S(s)$ and $C_T(s)$ determined by K_{DD_S}, K_{D_S}, K_{P_S}, K_{DD_T}, K_{D_T}, and K_{P_T} are chosen to match the frequency characteristic of the initial design in (10). Since the three denominator poles introduce some amount of phase lag in the vicinity of anticipated cross-over, additional compensatory phase lead is required by the zeros.

The matching of the frequency characteristics concentrates on the steady state gains, needed to achieve the desired performance (see [1, 2] for details), and on gain/phase relations around cross-over. In particular, robustness with respect to road adhesion μ dictates a region of phase lead for stabilization due to its influence on the overall vehicle gain. The PD-controllers of Section III provide approx. 90^o-phase lead up to the actuator bandwidth. For the controller structure (15), the phase lead region is selected such that a minimum of 60^o-phase lead is guaranteed at cross-over for $\mu \in [0.5,\ 1]$.

Last, the integral gain K_I is chosen to allow the fastest return to zero steady state tracking without interfering with stability, i.e. K_I is determined as large as possible, but not to introduce phase lag in the vicinity of the range of possible cross-over.

Manual parameter selection is followed by automated fine-tuning using the multi-objective optimization program (MOPS) provided within the control design software package AnDeCS© developed at DLR [17]. MOPS allows to optimize a vector of performance indices to be determined by the control designer. For the automatic steering control design problem, a combination of time domain and frequency domain criteria are chosen as performance indices. Time domain criteria include maximum lateral displacement and no overshoot for responses to step inputs of reference curvature according to Section II. Frequency domain criteria include minimal damping and "smoothness" of closed loop frequency curves to prevent excitation of single frequencies.

Since the vehicle dynamics vary dramatically with

driving speed v [1, 2], gain scheduling is designed with respect to speed. First, a high speed controller for $v^+ = 40$ m/s is derived using the described procedure. Second, v is gradually reduced and the above parameter optimization step is repeated without repeating any of the earlier control design steps. Last, gain scheduling laws of the form

$$K_S = K_{S_1} + \frac{K_{S_2}}{v} \quad \text{and} \quad K_T = K_{T_1} + K_{T_2} v \quad (16)$$

are synthesized for each controller parameter K_{P_S}, K_{I_S}, K_{D_S}, K_{DD_S}, and for K_{P_T}, K_{D_T}, and K_{DD_T}, respectively, in compliance with the variation of the vehicle dynamics with respect to speed v. In particular, the gain of the transfer function from steering angle δ to lateral acceleration features a v^ξ-dependency, with $\xi \approx 2$ for very low speed, $\xi \approx 1$ for normal US highway speed, and $0 < \xi < 1$ for very high speed. Gain scheduling (16) proved a suitable compromise to approximate this complex speed dependency.

V. Experimental Results

We have implemented and tested the above control design using the Pontiac 6000 STE Sedan , see Table 1. The test track consists of a straight section, a right turn followed by a left turn, another right turn and finally a straight section. The turning radii are $R_{ref} = 800$ m, without transitions in-between the curves to obtain step responses. Magnets [14] are installed at 1.2 m spacing over the full length of approx. 2 km. The car is equipped with magnetometers at the front and the rear bumpers as described above. Additionally, a gyroscope and a lateral accelerometer at CG are used to record the motion of the vehicle.

Curvature preview is encoded into the road using binary polarity coding of the magnets (similar to [18]). Dynamic curvature preview was added as feedforward control in some of the test runs. The preview steering angle is derived from the inverse of the second order vehicle lateral acceleration model at a virtual look-ahead point $d_V = \frac{K_{P_S} d_S + K_{P_T} d_T}{K_{P_S} - K_{P_T}}$. The integral gain K_I is set to zero initially in order to show pure step responses and steady state errors. Speed was kept at $v \approx 35$ m/s in the curved sections, which is equivalent to a lateral reference acceleration of $a_{ref} \approx 0.15$ g. The experimental results are show in Figures 5-8.

Figure 5 shows the controller performance on a dry road to be well damped without overshoot and within the accuracy specifications: The steady state error in the curves is approx. 0.2 m for $a_{ref} \approx 0.15$ g which is equivalent to errors of less than 0.15 m for $a_{ref} = 0.1$ g as specified in Section II. Using curvature preview and an integral term in Figure ?? eliminates the steady state tracking errors.

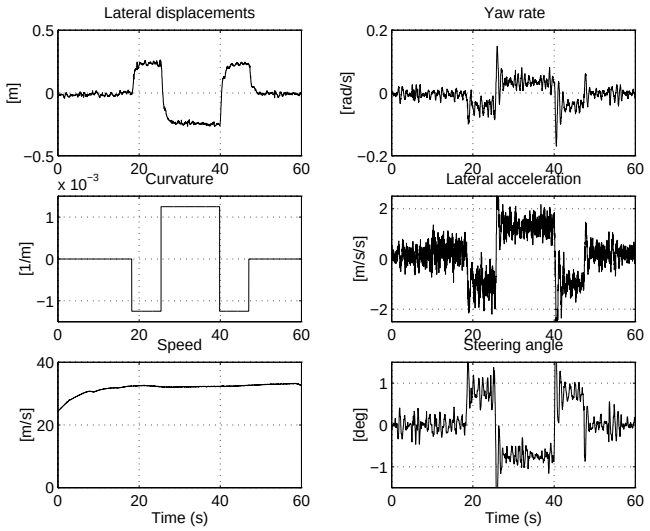

Fig. 5. Controller performance on dry road, without integral action and without road curvature preview

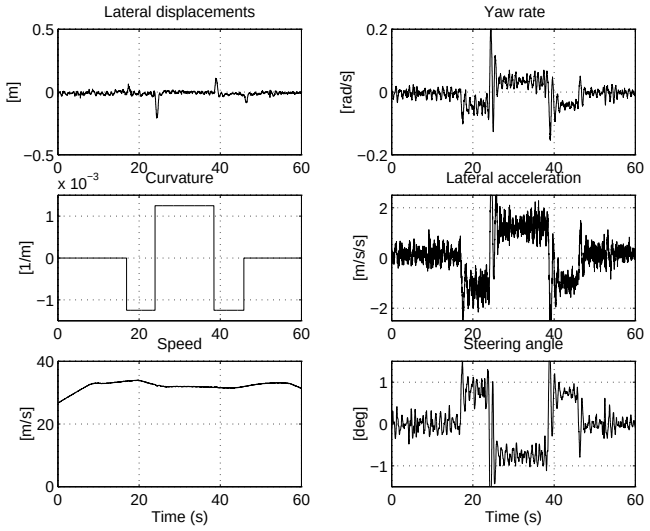

Fig. 6. Controller performance on dry road, with an integrator and with feedforward of road curvature

In order to simulate wet road, all controller gains were halved. This is equivalent to reducing road adhesion from $\mu = 1$ to $\mu = 0.5$, since such a deterioration would decrease the steady state gain of the lateral vehicle dynamics by approx. 40% (see also [1–3]). With controller gains reduced to 50% of their original values, steady state errors increased accordingly as shown in Figure ??, which are again eliminated when using curvature preview and integral action in Figure ??. Even at the points of reversing curvature with extreme steps of reference lateral acceleration of $a_{ref} \approx 0.3$ g, the maximum error was less than 0.2 m.

Ride comfort, a very subjective variable, was generally good except for the extreme curvature transitions with

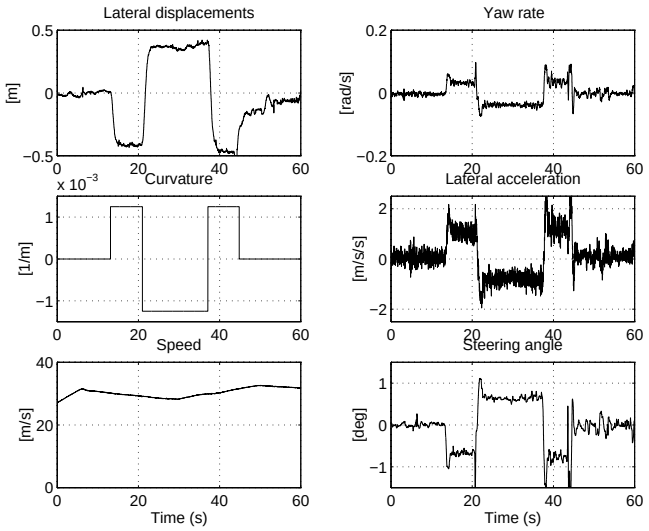

Fig. 7. Controller performance with halved gains to simulate a wet road, without integral action and without road curvature preview

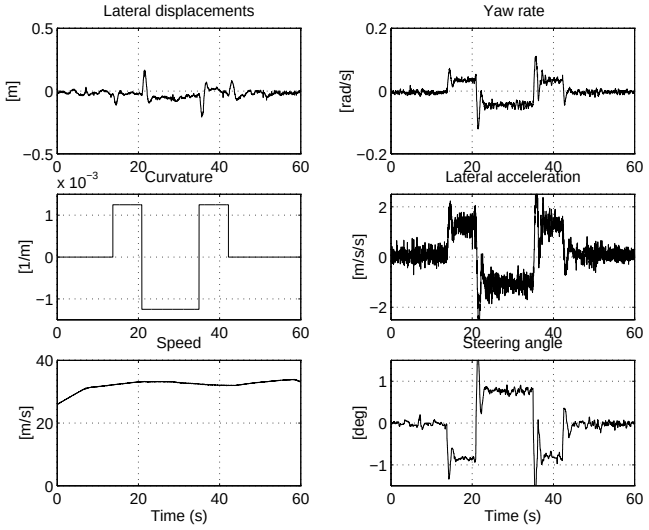

Fig. 8. Controller performance with halved gains to simulate a wet road, with an integrator and with feedforward of road curvature

$a_{ref} \approx 0.3$ g, were lateral jerk was noticeably too high. Such steps, however, will not appear on actual highways were the maximum curvature transition is $a_{ref} = 0.1$ g (on California Interstate highways). Noise in magnet installation and lateral displacement measurements triggered reactions of the automatic steering controller, visible in the plots for steering angle, and also in yaw rate and lateral acceleration. However, due to damping provided by the tires and the suspension, these small adjustments could not be felt by the passengers. It should be noted that the controller performance is a trade-off between accuracy and ride comfort. The presented controller structure, however, provides easy means to tune an appropriate compromise. The tracking errors for $v < 35$ m/s were smaller than the ones in Figures 5-8. However, in the experiments, the gains were not gain scheduled. Gain-scheduling may be used to achieve even smaller tracking errors at lower speed in order to accommodate sharper curves as prescribed in Section 4.2, e.g. for on-ramps and off-ramps of highways.

VI. Summary

Automatic steering control for passenger cars using look-down reference systems was restricted to speeds below highway speed in previously reported experimental approaches. To overcome these problems, an additional sensor for measuring the lateral vehicle displacement from the lane reference is introduced at the tail bumper to supplement the usually employed sensor at the front bumper. The additional tail sensor is one of the design directions proposed in [3] on the basis of a detailed system analysis.

In this paper, a robust control design was presented, incorporating practical constraints and limitations. In a first step, an initial controller based on state feedback of front and tail lateral displacement measurements and their derivatives was designed using the parameter space approach in an invariance plane. A second step refined the initial controller to output feedback without unmeasurable derivatives and accommodates practical considerations like accuracy and comfort. The performance and robustness of the control design was verified in an experimental test series at California Path. Experimental results confirmed the theoretical derivations and performance expectations.

References

[1] S. Patwardhan, H.-S. Tan, and J. Guldner, "A general framework for automatic steering control: System analysis", in *Proc. American Control Conf.*, Albuquerque, NM, USA, 1997, pp. 1598–1602.

[2] J. Guldner, H.-S. Tan, and S. Patwardhan, "Analysis of automatic steering control for highway vehicles with look-down lateral reference systems", *Vehicle System Dynamics*, vol. 26, no. 4, pp. 243–269, 1996.

[3] J. Guldner, H.-S. Tan, and S. Patwardhan, "On fundamental issues of vehicle steering control for highway automation", *Automatica*, submitted 1996.

[4] W. Stevens, "The automated highway system program: A progress report", in *Preprints of the 13th IFAC World Congress (plenary volume)*, San Francisco, CA, USA, 1996, pp. 25–34.

[5] S. Tsugawa, M. Aoki, A. Hosaka, and K. Seki, "A survey of present IVHS activities in Japan", in *Preprints of the 13th IFAC World Congress, Vol. Q*, San Francisco, CA, USA, 1996, pp. 147–152.

[6] M. Maurer *et al.*, "VaMoRs-P: An advanced platform for visual autonomous road vehicle guidance", in *Proc. SPIE Conf. 'Mobile Robots IX'*, Boston, 1994.

[7] B. Ulmer, "VITA - An autonomous road vehicle (ARV) for collision avoidance in traffic", in *Proc. of Intelligent vehicles '92*, Detroit, 1992, pp. 36–41.

[8] B. Ulmer, "VITA II - Active collision avoidance in real traffic", in *Proc. of Intelligent vehicles '94*, Paris, 1994, pp. 1–6.

[9] T. Jochem, D. Pomerleau, B. Kumar, and J. Armstrong, "PANS: A portable navigation platform", in *Proc. Intelligent vehicles Symposium*, Detroit, MI, USA, 1995, pp. 107–112.

[10] Q.-T. Luong, J. Weber, D. Koller, and J. Malik, "An integrated stereo-based approach to automatic vehicle guidance", in *Proc. of the 5th ICCV*, June 1995.

[11] K. A. Ünyelioğlu, C. Hatipoğlu, and Ü. Özgüner, "Design and stability analysis of a lane following controller", *IEEE Trans. on Control Systems Technology*, 1996.

[12] R. E. Fenton, G. C. Melocik, and K. W. Olson, "On the steering of automated vehicles: Theory and experiment", *IEEE Trans. on Automatic Control*, vol. 21, no. 3, pp. 306–315, 1976.

[13] W. Darenberg, "Automatische Spurführung von Kraftfahrzeugen (in German)", *Automobil-Industrie*, pp. 155–159, 1987.

[14] W. Zhang and R. E. Parsons, "An intelligent roadway reference system for vehicle lateral guidance/control", in *Proc. American Control Conf.*, San Diego, CA, USA, 1990, pp. 281–286.

[15] J. Ackermann, A. Bartlett, D. Kaesbauer, W. Sienel, and R. Steinhauser, *Robust control: Systems with uncertain physical parameters*, Springer, London, 1993.

[16] J. Ackermann and S. Türk, "A common controller for a family of plant models", in *Proc. 21st IEEE Conf. Decision and Control*, Orlando, 1982, pp. 240–244.

[17] G. Grübel, H. D. Joos, M. Otter, and R. Finsterwalder, "The ANDECS design environment for control engineering", in *Proc. 12th IFAC World Congress*, Sydney, Austr., 1993.

[18] J. Guldner, S. Patwardhan, H.-S. Tan, and W.-B. Zhang, "Coding of magnetic markers for demonstration of automated highway systems", in *Preprints of the Transportation Research Board Annual Meeting*, Washington, DC, USA, 1997.